Journal of Combinatorial Optimization (2026) 51:57
https://doi.org/10.1007/s10878-026-01435-2

Submodular Optimization for Heterogeneous UAV Deployment

Yang Lv[1] · Fengmin Wang[2] · Xiankun Yu[1] · Xin Li[1,3] · Dachuan Xu[1] · Ruiqi Yang[1]

Received: 19 December 2025 / Accepted: 15 May 2026
© The Author(s), under exclusive licence to Springer Science+Business Media, LLC, part of Springer Nature 2026

Abstract

Unmanned Aerial Vehicles (UAVs) are widely used in environmental monitoring tasks such as forest surveillance, agricultural mapping, and disaster assessment, where their ability to collect dense and high-resolution observations is particularly advantageous. However, many existing approaches implicitly assume that UAV platforms and onboard sensors are homogeneous. This assumption can introduce significant estimation errors in real-world deployments. This work studies the deployment of heterogeneous UAVs equipped with sensors of different accuracies for fire-scene assessment, using a point-of-interest–based model. Research on heterogeneous UAV measurements remains relatively limited. We introduce a weighted frame potential (WFP) that captures the orthogonality structure of sensing matrices under heterogeneous noise. By reformulating the problem as a submodular maximization task, we develop a Random Greedy Algorithm that guarantees a $1/(1+c)$ approximation of the optimal solution, where c denotes the curvature of the submodular function. A theoretical upper bound on the reconstruction error induced by the selected UAV configuration

✉ Ruiqi Yang
yangruiqi@bjut.edu.cn

Yang Lv
lvyang@emails.bjut.edu.cn

Fengmin Wang
casic_wfm@163.com

Xiankun Yu
22062213@emails.bjut.edu.cn

Xin Li
lixinyz@bjut.edu.cn

Dachuan Xu
xudc@bjut.edu.cn

1 Beijing Institute for Scientific and Engineering Computing, Beijing University of Technology, Beijing 100124, China

2 Jinghang Research Institute of Computing and Communication, Beijing 100074, China

3 College of Economics and Management, Beijing University of Technology, 100124 Beijing, China

Published online: 18 June 2026

is also established. Experiments on both small- and large-scale fire monitoring tasks show that the proposed method achieves higher reconstruction accuracy and better computational efficiency than existing algorithms.

Keywords UAV measurement · Approximation algorithm · Weighted frame potential · Submodular optimization

1 Introduction

UAVs have become increasingly important in environmental applications owing to their flexibility, maneuverability, and ability to carry various sensing payloads (Fang and Savkin 2024). They are widely used to gather heterogeneous data across different monitoring tasks. Despite these advantages, determining where UAVs should be positioned to ensure accurate and reliable sensing remains a key challenge.

To motivate this problem, we review advances in traditional sensor network research. Classical sensor networks (Ranieri et al. 2014; Bian et al. 2006; Li et al. 2021; Zhou et al. 2012; Rusu et al. 2017; Welch 1982; Krause et al. 2008; Jamali-Rad et al. 2014; Liu et al. 2014; Joshi and Boyd 2008; Chepuri and Leus 2014; Shamaiah et al. 2010; Jiang et al. 2016; Benedetto and Fickus 2003; Alonso et al. 2004; Mokhasi and Rempfer 2004) typically assume that all sensors operate independently and share identical characteristics. Within linear observation models designed for field reconstruction, a common objective is to choose k sensing locations from N candidates to maximize information gain or minimize estimation error. This leads to a combinatorial selection problem, prompting the development of numerous heuristic and approximation algorithms. Much of the existing work focuses on constructing criteria that quantify reconstruction error and designing algorithms that leverage the structure of these criteria (Li et al. 2021).

In contrast, relatively little attention has been paid to heterogeneous UAV sensing. In practice, UAV fleets often consist of platforms equipped with sensors of varying quality due to differences in manufacturing processes, acquisition times, or system configurations. As a result, measurement noise characteristics differ across UAVs, rendering the commonly adopted homogeneity assumption unrealistic and potentially inaccurate. Therefore, effectively coordinating UAVs with diverse sensing capabilities to obtain reliable measurements remains a challenging problem (Sultan et al. 2021).

We study how UAVs carrying sensors with different accuracy levels can jointly measure fire-impacted regions and reconstruct the underlying temperature field to locate hazardous areas. This framework also supports real-time wildfire alerting. In our setting, UAVs acquire measurements at predefined points of interest by hovering over these locations, and the collected observations are transmitted to a central processor that estimates the complete fire distribution, as shown in Figure 1. Each UAV type produces measurements corrupted by Gaussian noise with its own variance.

The objective is to devise a deployment strategy that assigns UAVs to measurement sites to minimize reconstruction error in a linear inverse formulation. Sensor heterogeneity introduces additional complexity, making conventional criteria such as mutual information or A-optimality inadequate, as they do not inherently reflect differences in

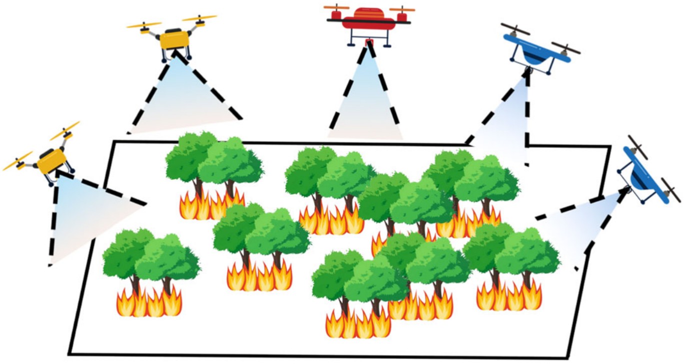

Fig. 1 Heterogeneous UAV Measurement Challenge: This figure illustrates a sensing scenario involving several UAV types. The fleet includes two yellow units, two blue units, and one red unit, each equipped with sensors of different accuracy. The goal is to determine an effective deployment strategy that minimizes measurement error during forest fire monitoring

sensor precision. To overcome this limitation, we introduce the weighted frame potential, which explicitly incorporates heterogeneous noise characteristics. The resulting metric is submodular, allowing the problem to be tackled using a random greedy approach. Submodularity ensures that this algorithm provides theoretical approximation guarantees while keeping computational costs low for large-scale scenarios.

The main contributions of this work are outlined below:

- We investigate environmental field reconstruction using heterogeneous UAV fleets, particularly when multiple UAV groups with different sensing characteristics are involved. Our results show that reliable collaborative sensing is still achievable despite variations in sensor quality and platform configuration.
- We propose a weighted frame potential metric that explicitly incorporates sensing heterogeneity, and we adopt a Random Greedy Algorithm that guarantees a $1/(1+c)$-approximation to the optimal solution, where c denotes the curvature of the submodular function. In addition, we develop a modified Random Greedy Algorithm that further improves empirical performance while preserving computational efficiency.

2 Related Prior Work

The UAV placement problem can be viewed as a generalization of the homogeneous sensor selection problem. The homogeneous sensor selection problem assumes that sensors are identical, while UAVs are heterogeneous and display varying noise distributions. However, even in the scenario of homogeneous sensors, the problem persists as an NP-hard issue (Bian et al. 2006). Direct enumeration through branch-and-bound methods can only accomplish sensor selection for extremely limited scenarios (Welch 1982). To effectively reduce measurement errors in applications, we review prior research from both criteria and algorithmic perspectives.

According to the summary in Li et al. (2021), the optimization problem for sensor placement involves three criteria: information-theoretic criteria, metric criteria, and data-driven criteria, all aimed at evaluating the effectiveness of sensor placement.

(1) Within the information-theoretic criteria, estimation vectors are modeled as Gaussian processes. By applying the entropy criterion (Zhou et al. 2012) and the mutual information criterion (Krause et al. 2008), sensors are strategically placed at locations with maximum variance, thereby reducing overall fitting errors. This method requires calculating the empirical mean and variance from available data. Although it achieves high fitting accuracy, it relies heavily on prior data.

(2) Within the metric criteria, Equation (2) represents a generalized linear model (Kay 1993). When sensors are appropriately selected, the physical field is accurately reconstructed. Various metrics are developed to optimize sensor placement based on different optimality criteria. The Mean Squared Error (MSE) metric, aligned with A-optimality, minimizes the average variance in the estimates of regression coefficients (Rusu et al. 2017; Jamali-Rad et al. 2014; Liu et al. 2014; Chepuri and Leus 2014). In contrast, the Worst Case Error Variance (WCEV) metric, associated with E-optimality, maximizes the minimum eigenvalue of the information matrix (Jiang et al. 2016; Alonso et al. 2004). The Log Volume of the Confidence Ellipsoid (VCE) metric, related to D-optimality, minimizes the volume of the η-confidence ellipsoid (Joshi and Boyd 2008; Chepuri and Leus 2014; Shamaiah et al. 2010). Fisher Information Intensity ensures a fair comparison of norms across different subspaces, avoiding the selection of positions solely based on the largest norm (Liu et al. 2023). Additionally, the Frame Potential (FP) metric, proposed by Benedetto and Fickus (2003), considers the orthogonality of selected row vectors to aid in identifying optimal solutions.

(3) Within the data-based criteria, a method based on maximizing the determinant of submatrices using column-pivoted QR decomposition is proposed for the sensor placement problem (Clark et al. 2018). Furthermore, Mokhasi and Rempfer (2004) utilizes a random forest algorithm to select input variables for optimal sensor placement, avoiding the theoretical complexities associated with optimization and POD algorithms.

Existing studies on heterogeneous UAV sensing mainly focus on capability coordination or task allocation, while rigorous deployment optimization with theoretical guarantees remains underexplored. Existing studies primarily focus on collaborative tasks involving UAVs with varying capabilities, such as sensor payloads (Lee et al. 2013; Berger et al. 2016) and flight performance (Chen et al. 2021). For instance, Majumder et al. (2025) investigates the use of weighted frame potential for linear inverse problems with heterogeneous sensors, but provides theoretical guarantees only for two UAV types under specific assumptions. Similarly, Zhang et al. (2018) proposes a scene reconstruction method that classifies sensors by precision, yet does not consider scenarios with a limited number of UAVs.

However, existing WFP-based methods typically capture only restricted forms of heterogeneity and often fail to enforce exact cardinality constraints across multiple sensor types. In contrast, our formulation accommodates arbitrary m-type heterogeneous UAVs under exact cardinality constraints, a setting that has not been addressed by existing WFP-based approaches.

3 PROBLEM STATEMENT

3.1 UAVs Model

For forest fire detection, UAVs are required to measure the affected region. As the objective is to minimize the WFP, larger measurement variances lead to poorer WFP values. On this plane, there are N candidate points, denoted by the set $\mathcal{N} = \{1, 2, \ldots, N\}$. In practical wildfire monitoring scenarios, there typically exist m types of heterogeneous UAVs. These UAVs differ in sensing capability, endurance, maneuverability, and terrain adaptability, and thus each type is more suitable for operation over specific areas. Accordingly, a candidate set $\mathcal{N}$ can be partitioned into m subsets $S_1, S_2, \ldots, S_m$, where each subset S_i corresponds to the set of locations that can be effectively accessed or observed by UAVs of type i, for $i = 1, 2, \ldots, m$. The objective of this study is to select a subset of candidate locations from the candidate set such that heterogeneous UAVs can be feasibly assigned to their corresponding regions.

In this setting, the number of available UAVs of each type is assumed to be known, and any feasible deployment plan $\mathcal{L} \subseteq \mathcal{N}$ must not exceed the capacity constraint of each UAV category. Specifically, if the available quantity of type-i UAVs is M_i, the solution must satisfy $|\mathcal{L} \cap S_i| = M_i$. Let L denote the set of deployed UAV locations. The total number of UAVs is given by $|\mathcal{L}| = L = \sum_{i=1}^{m} M_i$. Equivalently, all UAVs must be assigned to their designated subsets, and the total number of deployed units must exactly match the available inventory.

3.2 UAVs Placement Problem

Assume that our goal is to reconstruct the temperature at K selected points, whose true values are denoted by $\boldsymbol{\alpha} \in \mathbb{R}^K$. Following the sensing model in Jamali-Rad et al. (2014), the measurements collected at all candidate locations can be expressed as

$$\boldsymbol{f} = \Psi \boldsymbol{\alpha} + \boldsymbol{\eta}, \tag{1}$$

where $\Psi \in \mathbb{R}^{N \times K}$ characterizes the spatial relationship between the candidate measurement locations and the temperature reconstruction points, with more similar row vectors indicating spatially closer locations. The vector $\boldsymbol{\eta} \in \mathbb{R}^N$ represents additive measurement noise, modeled as zero-mean Gaussian white noise with covariance matrix $\mathbf{C}$.

The covariance matrix $\boldsymbol{C}$ takes a diagonal form and can be written as $\boldsymbol{C} = \mathbf{diag}(\sigma_1^2, \sigma_2^2, \ldots, \sigma_N^2)$. In this model, UAVs of the same type share the same measurement noise variance, and UAVs with higher sensing accuracy correspond to smaller variances. Let S_j denote the index set of UAVs belonging to the j-th type. For any $i \in S_j$, the noise variance σ_i^2 remains identical.

When the observation position set $\mathcal{L}$ for the UAVs is determined, the measurement vector obtained from these positions is denoted by $\boldsymbol{f}_{\mathcal{L}} \in \mathbb{R}^{|\mathcal{L}|}$, where $\boldsymbol{f}_{\mathcal{L}}$ represents the sub-vector of $\boldsymbol{f}$ indexed by $\mathcal{L}$. Similarly, $\boldsymbol{\eta}_{\mathcal{L}}$ denotes the corresponding noise sub-vector indexed by $\mathcal{L}$. The sub-matrix $\boldsymbol{\Psi}_{\mathcal{L}} \in \mathbb{R}^{|\mathcal{L}| \times K}$ is composed of the rows of $\boldsymbol{\Psi}$

indexed by $\mathcal{L}$. Based on these definitions, the sensing model restricted to the location set $\mathcal{L}$ can be written as

$$\boldsymbol{f}_{\mathcal{L}} = \boldsymbol{\Psi}_{\mathcal{L}}\boldsymbol{\alpha} + \boldsymbol{\eta}_{\mathcal{L}}. \tag{2}$$

Due to the limited number of UAVs, it is impossible to cover all selected points. As a result, the measurement vector $\boldsymbol{f}_{\mathcal{L}}$ has a smaller dimension than the full measurement vector $\boldsymbol{f}$. This reduction in dimensionality adversely affects the accurate recovery of $\boldsymbol{\alpha}$. Therefore, the central challenge of this paper is how to effectively leverage a limited fleet of heterogeneous UAVs to enhance the reconstruction of $\boldsymbol{\alpha}$.

3.3 Weighted Frame Potential (WFP)

In temperature reconstruction tasks, various criteria are commonly employed to evaluate the effectiveness of the selected reference set. Prior studies have introduced several metrics, such as MSE (Jiang et al. 2019), VCE (Shamaiah et al. 2010), and WCEV (Jiang et al. 2016). Benedetto and Fickus (2003) proposed an approach based on the notion of frame potential. Building on this foundation, subsequent work extended the original frame potential to accommodate heterogeneous settings, leading to the concept of the weighted frame potential.

Let $\mathcal{L}$ denote the selected index set. Define $\boldsymbol{\Psi}_{\mathcal{L}}$ as the submatrix consisting of the rows indexed by $\mathcal{L}$, and let $\boldsymbol{\psi}_i$ denote the i-th row of $\boldsymbol{\Psi}_{\mathcal{L}}$. The weighting coefficients are given by $\omega_i = \sigma_i$, where σ_i denotes the standard deviation of the measurement noise at location i. The weighted frame potential is defined as

$$WFP(\boldsymbol{\Psi}_{\mathcal{L}}) = \sum_{i,j\in\mathcal{L}} \omega_i\omega_j \frac{\langle \boldsymbol{\psi}_i, \boldsymbol{\psi}_j \rangle^2}{\|\boldsymbol{\psi}_i\| \cdot \|\boldsymbol{\psi}_j\|}. \tag{3}$$

The weighted frame potential quantifies the overall correlation among the selected row vectors, and a smaller value generally indicates a more desirable choice.

Since the primary objective is to minimize the WFP, larger variances in UAV measurement errors naturally correspond to poorer values of the WFP metric. This suggests increasing the associated weighting factors ω_i. For scenarios involving multiple UAV groups, empirical results indicate that setting $\omega_i = \sigma_i$ leads to consistently strong performance. Assigning each ω_i to be the standard deviation corresponding to index i leads to superior outcomes.

Minimizing the WFP presents significant challenges in algorithm design. To address this, a monotone, normalized, and submodular function f is constructed. The core principle behind constructing f is to identify the complement of the solution set and exclude row vectors that minimally decrease the value of WFP. These positions are deemed unsuitable for UAV placement. Through this construction, the function f becomes

$$f(\mathcal{L}) = WFP(\boldsymbol{\Psi}_{\mathcal{N}}) - WFP(\boldsymbol{\Psi}_{\mathcal{N}\setminus\mathcal{L}}). \tag{4}$$

Lemma 1 *The set function $f : 2^{\mathcal{N}} \to \mathbb{R}$ is normalized, monotone, and submodular.*

Proof We first verify the normalization property. When $\mathcal{L} = \emptyset$, it follows that

$$
\begin{aligned}
f(\emptyset) &= WFP(\boldsymbol{\Psi}_{\mathcal{N}}) - WFP(\boldsymbol{\Psi}_{\mathcal{N}\setminus\emptyset}) \\
&= WFP(\boldsymbol{\Psi}_{\mathcal{N}}) - WFP(\boldsymbol{\Psi}_{\mathcal{N}}) \\
&= 0,
\end{aligned} \tag{5}
$$

which confirms that f is normalized.

Next, we establish monotonicity. From the definition of WFP in (3), each summation term is nonnegative, and adding more elements to the index set increases the number of terms in the summation. Hence, $WFP(\boldsymbol{\Psi}_{\mathcal{A}})$ is monotonically increasing with respect to $\mathcal{A}$. Consequently, its complement $WFP(\boldsymbol{\Psi}_{\mathcal{N}\setminus\mathcal{L}})$ is monotonically decreasing, and therefore

$$
f(\mathcal{L}) = WFP(\boldsymbol{\Psi}_{\mathcal{N}}) - WFP(\boldsymbol{\Psi}_{\mathcal{N}\setminus\mathcal{L}})
$$

is monotonically increasing.

We now prove the submodularity of f. Consider two sets $\mathcal{L}_1 \subseteq \mathcal{L}_2 \subseteq \mathcal{N}$ and an element $e \notin \mathcal{L}_2$. We compare the marginal gains obtained by adding e to these two sets.

From the definition of f, we have

$$
\begin{aligned}
f(\mathcal{L}_1 \cup \{e\}) - f(\mathcal{L}_1) &= WFP(\boldsymbol{\Psi}_{\mathcal{N}\setminus\mathcal{L}_1}) - WFP(\boldsymbol{\Psi}_{\mathcal{N}\setminus(\mathcal{L}_1\cup\{e\})}) \\
&= \sum_{i\in\mathcal{N}\setminus(\mathcal{L}_1\cup\{e\})} \omega_i\omega_e \frac{\langle \boldsymbol{\psi}_i, \boldsymbol{\psi}_e\rangle^2}{\|\boldsymbol{\psi}_i\|_2 \, \|\boldsymbol{\psi}_e\|_2} \; + \; \omega_e^2.
\end{aligned} \tag{6}
$$

Similarly, the marginal gain of adding e to $\mathcal{L}_2$ is given by

$$
f(\mathcal{L}_2 \cup \{e\}) - f(\mathcal{L}_2) = \sum_{i\in\mathcal{N}\setminus(\mathcal{L}_2\cup\{e\})} \omega_i\omega_e \frac{\langle \boldsymbol{\psi}_i, \boldsymbol{\psi}_e\rangle^2}{\|\boldsymbol{\psi}_i\|_2 \, \|\boldsymbol{\psi}_e\|_2} \; + \; \omega_e^2. \tag{7}
$$

Since $\mathcal{L}_1 \subseteq \mathcal{L}_2$, it follows that

$$
\mathcal{N} \setminus (\mathcal{L}_2 \cup \{e\}) \subseteq \mathcal{N} \setminus (\mathcal{L}_1 \cup \{e\}).
$$

Moreover, all summands in the above expressions are nonnegative and independent of the choice of $\mathcal{L}_1$ and $\mathcal{L}_2$. Therefore, the marginal gain obtained by adding e decreases as the conditioning set grows, i.e.,

$$
f(\mathcal{L}_1 \cup \{e\}) - f(\mathcal{L}_1) \;\geq\; f(\mathcal{L}_2 \cup \{e\}) - f(\mathcal{L}_2).
$$

This establishes the diminishing returns property, and hence f is submodular.

In summary, we have shown that f is normalized, monotone, and submodular. These properties enable the design of an efficient approximation algorithm for maximizing f. □

4 Algorithm and Theoretical Foundations

In this section, the heterogeneous UAV placement problem is addressed by formulating it as a submodular maximization problem. We employ the Random Greedy Algorithm, which is not only straightforward to implement but also provides clean theoretical performance guarantees.

4.1 Algorithm

The function f is normalized, monotone, and submodular. Let M_i denote the number of UAVs belonging to the i-th type. We define $\mathcal{L}'$ as the set of locations to be excluded from UAV deployment. The corresponding constraint can be written as

$$|(\mathcal{N} \setminus \mathcal{L}') \cap S_i| = M_i.$$

If $|S_i|$ denotes the cardinality of S_i, this constraint is equivalent to

$$|\mathcal{L}' \cap S_i| = |S_i| - M_i.$$

For convenience, define $M_i' = |S_i| - M_i$, and let $L' = \sum_{i=1}^{m} M_i'$. The optimization problem can then be formulated as

$$\begin{aligned} &\arg\max_{\mathcal{L}' \subseteq \mathcal{N}} \; f(\mathcal{L}'), \\ &\text{s.t.} \quad |\mathcal{L}' \cap S_i| = M_i', \quad i = 1, \ldots, m. \end{aligned} \tag{8}$$

When $m = 1$, the problem reduces to maximizing a submodular function under a uniform matroid constraint (Nemhauser et al. 1978). In this classical setting, the greedy algorithm achieves a $(1 - 1/e)$-approximation of the optimal solution. We next extend this framework to the more general case where m is an arbitrary constant.

Conforti and Cornuéjols (1984) introduce the notion of curvature c for submodular functions and analyze its impact on the performance of the greedy algorithm. The curvature quantifies how far a submodular function deviates from linearity. When $c = 0$, the greedy algorithm is optimal; when $c \in [0, 1)$, its approximation ratio improves beyond the classic $1/2$ guarantee; and when $c = 1$, the bound matches the classical worst-case approximation factor. The curvature has since become a fundamental tool in subsequent research on submodular optimization. It is defined as

$$c = 1 - \min_{i \in \mathcal{N}} \frac{f(\mathcal{N}) - f(\mathcal{N} \setminus \{i\})}{f(\{i\})}.$$

Similar curvature-based refinements have also appeared in more general submodular maximization settings (Lv et al. 2024).

We address this problem using a greedy strategy. We first employ a Random Greedy Algorithm to establish the theoretical guarantees of our method. We introduce a modified Random Greedy Algorithm to achieve better empirical performance.

Algorithm 1 Random Greedy Algorithm for Submodular Maximization

Require: Submodular function $f : 2^{\mathcal{N}} \to \mathbb{R}$, ground sets $S_1, S_2, \ldots, S_m$, and selection limits $M_1', M_2', \ldots, M_m'$

Construct a multi-element index list $\mathcal{I}$ that contains M_1' copies of index 1, M_2' copies of index 2, ..., and M_m' copies of index m. {This list determines the randomized order of which category of UAVs to select from.}

Randomly permute the list $\mathcal{I}$.

$\mathcal{L}' \leftarrow \emptyset$

for each index j in the permuted list $\mathcal{I}$ **do**

  $i \leftarrow \arg\max_{i \in S_j} \left\{ f(\mathcal{L}' \cup \{i\}) - f(\mathcal{L}') \right\}$

  $\mathcal{L}' \leftarrow \mathcal{L}' \cup \{i\}$

end for

return $\mathcal{L}'$

The pseudocode of the Random Greedy Algorithm is given in Algorithm 1. Before the algorithm starts, the elements to be selected are random by independently shuffling the M_1' elements drawn from S_1, the M_2' elements drawn from S_2, and so on. In each iteration, the algorithm selects the element with the largest marginal gain from the current partition.

4.2 Algorithm Approximation Guarantee

Lemma 2 *Let $f : 2^{\mathcal{N}} \to \mathbb{R}$ be a normalized, monotone, and submodular function with curvature c. When maximizing f under a partition matroid constraint, Algorithm 1 achieves an approximation ratio of* $1/(1+c)$.

Proof Let OPT denote the optimal solution, and define

$$OPT_1 = OPT \cap S_1, \quad OPT_2 = OPT \cap S_2, \ \ldots, \ OPT_m = OPT \cap S_m.$$

Thus, OPT_i contains exactly the M_i' elements of OPT that lie in S_i. For any intermediate solution T, let T_i denote the set obtained after the i-th iteration of the algorithm.

Since OPT is a feasible solution under the partition matroid constraint, it must satisfy $|OPT_i| = M_i'$ for all $i = 1, \ldots, m$.

Bijection Construction. For each group S_j, we construct a bijection between $T \cap S_j$ and OPT_j. If $e_j \in (T \cap S_j) \cap OPT_j$, we map e_j to itself. For the remaining elements, i.e., those in $(T \cap S_j) \setminus OPT_j$, we randomly define a bijection onto the set $OPT_j \setminus (T \cap S_j)$. Hence, every $i \in T \cap S_j$ is paired with a unique $o_i^j \in OPT_j$.

We now show that $f(i \mid T_{i-1}) \geq f(o_i^j \mid T_{i-1})$. If $i \in OPT_j$, then $i = o_i^j$, and the inequality is trivial. If $i \notin OPT_j$, then in the i-th iteration the greedy rule selected i while o_i^j was available but not chosen, which implies $f(i \mid T_{i-1}) \geq f(o_i^j \mid T_{i-1})$.

Bounding. By submodularity of f, we have

$$\begin{aligned} f(OPT \cup T) &\leq f(T) + \sum_{j=1}^{m} \sum_{o_i \in OPT_j} f\big(o_i \mid T_{i-1}\big) \\ &\leq f(T) + \sum_{j=1}^{m} \sum_{i \in T \cap S_j} f\big(i \mid T_{i-1}\big), \end{aligned} \tag{9}$$

where the second inequality follows directly from the bijections constructed above.

Next, using telescoping expansion over elements of T and applying the curvature bound, we obtain

$$\begin{aligned} f(OPT \cup T) &= f(OPT) + \sum_{j=1}^{m} \sum_{i \in T \cap S_j} f\big(i \mid OPT \cup T_{i-1}\big) \\ &\geq f(OPT) + (1-c) \sum_{j=1}^{m} \sum_{i \in T \cap S_j} f\big(i \mid T_{i-1}\big). \end{aligned} \tag{10}$$

Putting the two inequalities together yields

$$f(OPT) \;\leq\; f(T) + c \sum_{j=1}^{m} \sum_{i \in T} f\big(i \mid T_{i-1}\big) \;=\; (1+c)\, f(T). \tag{11}$$

Thus, the value returned by Algorithm 1 achieves at least a $1/(1+c)$ fraction of the optimal value, proving the claimed approximation ratio. □

Theorem 1 *Consider any heterogeneous UAV placement problem, and let*

$$OPT = \arg \max_{\mathcal{A} \subseteq \mathcal{N},\, |\mathcal{A} \cap S_i| = M_i} f(\mathcal{A}) \tag{12}$$

denote the optimal solution. We assume that the UAV placement strategy corresponding to the optimal solution satisfies $\mathcal{N} \setminus OPT = \overline{OPT}$. *Let* $\mathcal{N} \setminus T$ *be the suboptimal solution returned by the greedy algorithm. Then the corresponding matrices* $\boldsymbol{\Psi}_{\mathcal{N} \setminus T}$ *and* $\boldsymbol{\Psi}_{\overline{OPT}}$ *satisfy*

$$WFP\big(\boldsymbol{\Psi}_{\mathcal{N} \setminus T}\big) \;\leq\; \gamma\, WFP\big(\boldsymbol{\Psi}_{\overline{OPT}}\big), \tag{13}$$

where

$$\gamma = 1 + \frac{c \cdot WFP(\boldsymbol{\Psi})}{L_{\min}} \tag{14}$$

is the approximation factor, and

$$L_{\min} = \min_{|\mathcal{L}'| = L'} \left(\sum_{i,j \in \overline{OPT}} \omega_i \omega_j \frac{\langle \boldsymbol{\psi}_i, \boldsymbol{\psi}_j \rangle^2}{\|\boldsymbol{\psi}_i\|_2 \, \|\boldsymbol{\psi}_j\|_2} \right). \tag{15}$$

Proof Since the greedy algorithm guarantees

$$f(T) \geq \frac{1}{1+c} f(OPT),$$

and since OPT is arbitrary among all feasible solutions, we substitute $OPT = \mathcal{N} \setminus \overline{OPT}$, which is also feasible, to obtain

$$WFP(\boldsymbol{\Psi}) - WFP\big(\boldsymbol{\Psi}_{\mathcal{N}\setminus\mathcal{L}'}\big) \geq \frac{1}{1+c}\Big(WFP(\boldsymbol{\Psi}) - WFP\big(\boldsymbol{\Psi}_{\overline{OPT}}\big)\Big). \tag{16}$$

Rearranging terms gives

$$WFP\big(\boldsymbol{\Psi}_{\mathcal{N}\setminus\mathcal{L}'}\big) \leq \frac{1}{1+c}\left(1 + \frac{c \cdot WFP(\boldsymbol{\Psi})}{WFP(\boldsymbol{\Psi}_{\overline{OPT}})}\right) WFP\big(\boldsymbol{\Psi}_{\overline{OPT}}\big). \tag{17}$$

Since

$$WFP\big(\boldsymbol{\Psi}_{\overline{OPT}}\big) = \sum_{i,j\in\overline{OPT}} \omega_i \omega_j \frac{\langle \boldsymbol{\psi}_i, \boldsymbol{\psi}_j \rangle^2}{\|\boldsymbol{\psi}_i\|_2 \, \|\boldsymbol{\psi}_j\|_2}, \tag{18}$$

We derive a lower bound by minimizing the squared sum over all subsets of size $\mathcal{L}$, leading to

$$\sum_{i,j\in\overline{OPT}} \omega_i \omega_j \frac{\langle \boldsymbol{\psi}_i, \boldsymbol{\psi}_j \rangle^2}{\|\boldsymbol{\psi}_i\|_2 \, \|\boldsymbol{\psi}_j\|_2} \geq \min_{|\mathcal{L}|=L'} \left(\sum_{i,j\in\overline{OPT}} \omega_i \omega_j \frac{\langle \boldsymbol{\psi}_i, \boldsymbol{\psi}_j \rangle^2}{\|\boldsymbol{\psi}_i\|_2 \, \|\boldsymbol{\psi}_j\|_2} \right) = L_{\min}. \tag{19}$$

Based on (19), we obtain the inequality

$$\begin{aligned} WFP\big(\boldsymbol{\Psi}_{\mathcal{N}\setminus\mathcal{L}}\big) &\leq \frac{1}{1+c}\left(1 + \frac{c \cdot WFP(\boldsymbol{\Psi})}{WFP\big(\boldsymbol{\Psi}_{\overline{OPT}}\big)}\right) WFP\big(\boldsymbol{\Psi}_{\overline{OPT}}\big) \\ &\leq \frac{1}{1+c}\left(1 + \frac{c \cdot WFP(\boldsymbol{\Psi})}{L_{\min}}\right) WFP\big(\boldsymbol{\Psi}_{\overline{OPT}}\big). \end{aligned} \tag{20}$$

□

This establishes the theoretical guarantee for the upper bound of the approximation algorithm's performance measured by the WFP metric. As the values of the WFP in $\boldsymbol{\Psi}_{\mathcal{N}\setminus\mathcal{L}'}$ decrease, $\boldsymbol{\Psi}_{\mathcal{N}\setminus\mathcal{L}'}$ approaches orthogonality, resulting in a smaller error.

4.3 Heuristic Enhancement: Modified Random Greedy Algorithm

The approximation guarantee established relies on the curvature c of the submodular function and applies strictly to Algorithm 1. In practice, however, we observe that the empirical performance of greedy-type algorithms is often limited by strong correlations among selected sensing vectors, which may lead to large effective curvature.

Motivated by this observation, we introduce a Modified Random Greedy Algorithm (MRGA) as a heuristic enhancement of Algorithm 1. The MRGA is not intended to optimize a strictly submodular objective, nor does it admit the same worst-case approximation guarantees. Instead, it aims to empirically reduce redundancy among selected sensing vectors and thereby improve reconstruction accuracy in practical deployments.

The following lemma does not establish a new approximation bound for MRGA. Instead, it provides theoretical insight into how correlations among sensing vectors affect the curvature, thereby motivating the design of correlation-aware heuristics.

Lemma 3 *For a submodular function f, its curvature c is upper-bounded by a quantity that increases monotonically with*

$$\max_{i\in\mathcal{N}} \frac{2}{\omega_i\|\psi_i\|} \sum_{j\in\mathcal{N}\setminus\{i\}} \frac{\omega_j\langle\psi_i,\psi_j\rangle^2}{\|\psi_j\|}.$$

Proof

$$\begin{aligned} c &= 1-\min_{i\in\mathcal{N}} \frac{f(\mathcal{N})-f(\mathcal{N}\setminus\{i\})}{f(\{i\})} = 1-\min_{i\in\mathcal{N}} \frac{WFP(\boldsymbol{\Psi}_{\{i\}})}{WFP(\boldsymbol{\Psi}_{\mathcal{N}})-WFP(\boldsymbol{\Psi}_{\mathcal{N}\setminus\{i\}})} \\ &= 1-\min_{i\in\mathcal{N}} \frac{\omega_i^2}{\omega_i^2+\frac{2\omega_i}{\|\psi_i\|}\sum_{j\in\mathcal{N}\setminus\{i\}}\frac{\omega_j\langle\psi_i,\psi_j\rangle^2}{\|\psi_j\|}} \\ &= 1-\min_{i\in\mathcal{N}} \frac{1}{1+\frac{2}{\omega_i\|\psi_i\|}\sum_{j\in\mathcal{N}\setminus\{i\}}\frac{\omega_j\langle\psi_i,\psi_j\rangle^2}{\|\psi_j\|}}. \end{aligned}$$

This expression provides the claimed form of the curvature. □

This lemma provides the following insight: the approximation ratio worsens when the term $\frac{2}{w_i\|\psi_i\|}\sum_{j\in\mathcal{N}\setminus\{i\}}\frac{w_j\langle\psi_i,\psi_j\rangle^2}{\|\psi_j\|}$ is large. In geometric terms, this corresponds to ψ_i and ψ_j being almost collinear, meaning the two sensing vectors are strongly correlated. Such correlation increases the effective curvature of the objective, thereby weakening the approximation guarantee. To mitigate this effect and improve overall performance, it is desirable to avoid selecting elements whose sensing vectors are closely aligned with those already chosen.

Guided by this observation, we enhance the random greedy procedure by incorporating an additional penalization mechanism. As illustrated in Algorithm 2, rather than selecting the candidate that provides the maximum marginal gain $f(T\cup\{i\})-f(T)$, we modify the scoring rule to penalize candidates whose feature vectors are strongly

Algorithm 2 Modified Random Greedy Algorithm for Submodular Maximization

Require: Submodular function $f : 2^{\mathcal{N}} \to \mathbb{R}$, partition blocks $S_1, S_2, \ldots, S_m$, and selection limits $M'_1, M'_2, \ldots, M'_m$

1: Construct an index list $\mathcal{I}$ containing M'_1 copies of index 1, M'_2 copies of index 2, …, M'_m copies of index m {This list determines the randomized order of which category of UAVs to select from.}
2: Randomly permute $\mathcal{I}$
3: $\mathcal{L}' \leftarrow \emptyset$
4: **for** each index j in the permuted list $\mathcal{I}$ **do**
5: Select

$$i = \arg\max_{i \in S_j} \left\{ f(\mathcal{L}' \cup \{i\}) - f(\mathcal{L}') \; - \; \frac{\lambda}{w_i \|\psi_i\|} \sum_{j \in \mathcal{L}'} \frac{w_j \langle \psi_i, \psi_j \rangle^2}{\|\psi_j\|}, \right\}$$

6: $\mathcal{L}' \leftarrow \mathcal{L}' \cup \{i\}$
7: **end for**
8: **return** $\mathcal{L}'$

aligned with the current aggregate direction. More precisely, each candidate i is evaluated using

$$f(T \cup \{i\}) - f(T) \; - \; \frac{\lambda}{w_i \|\psi_i\|} \sum_{j \in T} \frac{w_j \langle \psi_i, \psi_j \rangle^2}{\|\psi_j\|},$$

where λ is a tunable parameter, set to 0.1 in our implementation. This modification reduces directional redundancy, effectively lowering curvature and improving empirical performance in UAV placement tasks.

5 Numerical Results

In this section, we evaluate the performance of the two proposed algorithms, the Random Greedy Algorithm (RGA) and the Modified Random Greedy Algorithm (MRGA), and compare them against several benchmark methods reported in the literature. Numerical experiments are conducted under both small-scale and large-scale settings to validate the effectiveness of the proposed approaches.

5.1 Small-Scale UAV Measurements

In the small-scale scenario, we compare the performance of the RGA and MRGA with three additional algorithms described as follows:

Random Greedy Algorithm (RGA): The WFP and the Random Greedy Algorithm are employed to identify the set of points where UAVs cannot be placed, after which the feasible set is obtained by taking their complement. In each iteration, the Random Greedy Algorithm selects a category uniformly at random and removes one element from it. The final solution satisfies all prescribed constraints.

Modified Random Greedy Algorithm (MRGA): Unlike the RGA, the MRGA prioritizes selecting mutually uncorrelated points when determining the set of locations where UAVs cannot be placed. This strategy reduces the resulting curvature c.

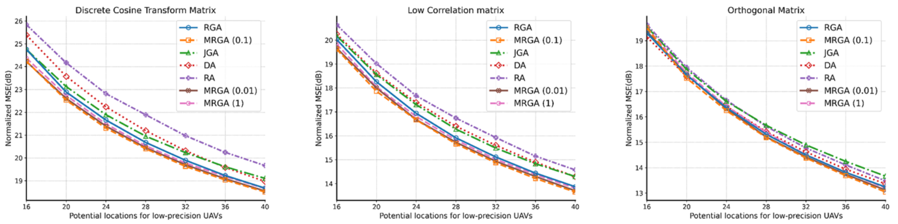

Fig. 2 The number of low-precision UAVs varies from 16 to 40, and the corresponding reconstruction errors obtained by different algorithms are compared

Joint Greedy Algorithm (JGA) (Majumder et al. 2025): The algorithm selects, from all feasible candidate points, the one with the largest potential value that does not violate the constraints, and then determines its complement as the UAV placement set. Its theoretical upper bound is identical to that of the RGA.

Determinant Algorithm (DA) (Joshi and Boyd 2008): The UAV selection process is performed in stages according to different accuracy levels. At each step, the algorithm identifies the index j that yields the maximum marginal gain, given by

$$\log\det\left(\overline{\sigma}^{-2}\sum_{i\in S}\boldsymbol{\psi}_i\tilde{\boldsymbol{\psi}}_i+\boldsymbol{\psi}_j\tilde{\boldsymbol{\psi}}_j+\boldsymbol{\Sigma}^{-1}\right).$$

This approach depends solely on the value of $\overline{\sigma}$ and does not capture the heterogeneity present among different UAVs.

Random Algorithm (RA): For each category of UAV placements, a feasible point satisfying the problem requirements is selected uniformly at random to form the UAV deployment set.

We choose $\boldsymbol{\Psi}^{130\times 15}$ using three different approaches: the discrete cosine transform matrix, the low correlation matrix, and the orthogonal matrix. There are three different models of UAVs, denoted as $m = 3$. These three distinct UAVs are assigned measurement missions. The first type comprises 2 high-precision UAVs with 20 potential locations. The Gaussian noise variance is set at 0.01. The second type includes 5 medium-precision UAVs with 30 potential locations and a noise variance of 0.1. Lastly, the third type involves 80 low-precision UAVs with potential locations ranging from 16 to 40. These UAVs have a noise variance of 0.3. The goal is to place the UAVs at the potential locations in a manner that minimizes their errors. The evaluation metric is MSE, and we consider 100 randomly generated examples to calculate the average MSE as the outcome of the experiment.

The line chart in Figure 2 illustrates the impact of measurement errors for low-precision UAVs, where the number of such UAVs varies from 16 to 40. Figure 3 reports the runtime of each algorithm. Due to differences in matrix operations, only the discrete cosine transform matrix is presented for visualization. The results show that the mean square error decreases as the number of low-precision UAVs increases. Among the five algorithms considered, the RGA and MRGA exhibit superior performance across all three matrices. The runtime of the DA algorithm grows as more sensors are selected, whereas the greedy-type algorithms remain relatively stable. The RGA, MRGA, and

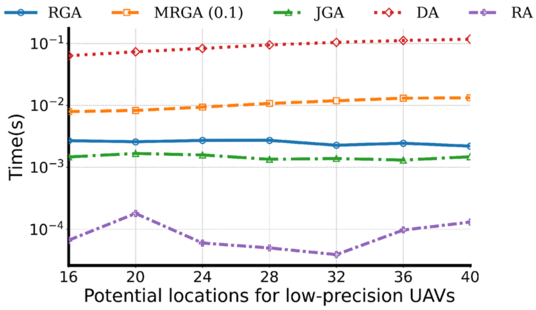

Fig. 3 The number of low-precision UAVs deployed ranges from 16 to 40, and the computation time varies with different algorithms

JGA are all greedy algorithms and therefore maintain relatively low computational complexity. In contrast, the DA algorithm requires determinant evaluations and is approximately three hundred times slower than the greedy algorithms. This trend becomes even more pronounced in large-scale scenarios. For dynamic environments and applications that require rapid responses, algorithms with high computational efficiency are more suitable for practical deployment.

For the choice of λ, experimental results indicate that the algorithm performs best when $\lambda = 0.1$, with slightly worse performance when $\lambda = 0.01$, and even poorer performance when $\lambda = 1$. This demonstrates that selecting an appropriate value for λ is crucial for the algorithm's performance, and a proper choice of this parameter can significantly enhance the optimization results.

5.2 Large-Scale Fire Disaster Rescue Problem

In large-scale fire scenarios, the rapid deployment of UAVs for disaster-site observation is of critical importance. The selected area for fire monitoring covers a region of 1 km by 2 km, where the average temperature ranges from 30 to 400 degrees Celsius. The underlying fire field is generated through interpolation of regression-based estimates obtained from a collection of sampled points. As shown in Figure 4, the spatial distribution of the simulated fire exhibits two distinct high-temperature regions. An effective algorithm should aim to capture these hotspots with high accuracy.

In this setting, two categories of UAVs are deployed. The first category consists of twenty UAVs with eighty potential locations, and the second category consists of fifty-five UAVs with two hundred potential locations. Their measurement variances are set to two and six respectively. To reconstruct the fire field, the UAVs collect temperature observations at seventy-five representative points distributed across the region of interest. The complete fire scene is then approximated through spatial interpolation. The sensing matrix $\boldsymbol{\Psi}$ is constructed as a 280×75 matrix, obtained as a submatrix of a two hundred and eighty dimensional orthogonal basis. For the algorithmic comparison, only the RGA, MRGA, JGA, DA, and RA methods considered in this study are included in the evaluation.

The algorithmic results reveal that the execution times for RGA, MRGA, JGA, DA, and RA are 0.007s, 0.023s, 0.007s, 5.651s, and 0.001s, respectively. It can be observed that both RGA and MRGA maintain low execution times, while DA experiences a

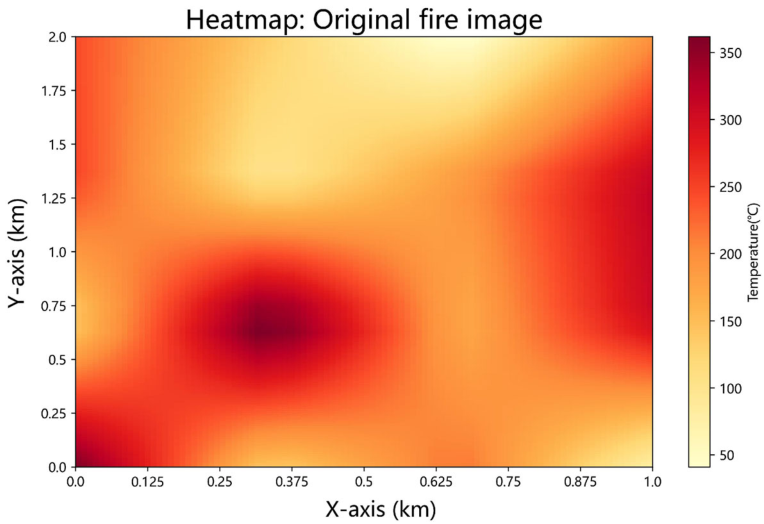

Fig. 4 Simulated fire scene heatmap over an area of 2 km by 1 km

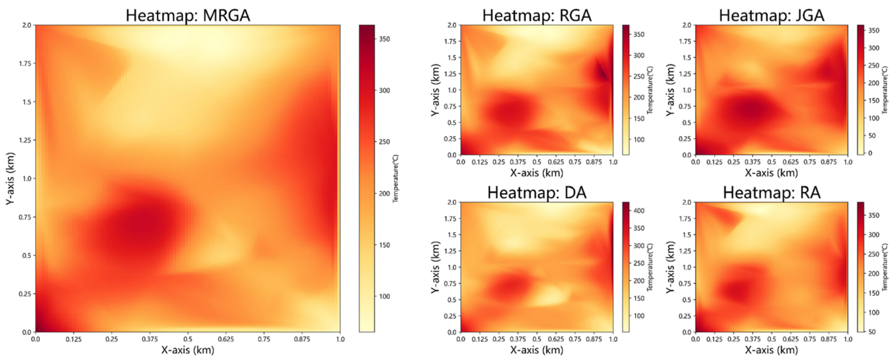

Fig. 5 Interpolated fire scene plots provided by the five algorithms. The large panel on the left corresponds to the MRGA, while the four panels on the right correspond to the RGA (top left), JGA (top right), DA (bottom left), and RA (bottom right)

sharp increase in runtime due to the high time complexity associated with determinant calculations. Therefore, DA is not a favorable choice for large-scale scenarios, as its performance significantly degrades in such cases.

The measurement outcomes produced by the algorithms are interpolated to obtain the reconstructed fire scenes shown in Figure 5. From a visual perspective, the reconstruction generated by the MRGA in the left panel is the most accurate. It successfully identifies the two high-temperature hotspots and maintains smooth transitions across the intermediate regions. The RGA also captures the two hotspots, although its reconstruction is less refined compared to that of the MRGA. The inferior performance observed in the remaining algorithms can be attributed to inaccuracies in their measurement estimates, which negatively affect the quality of the interpolation.

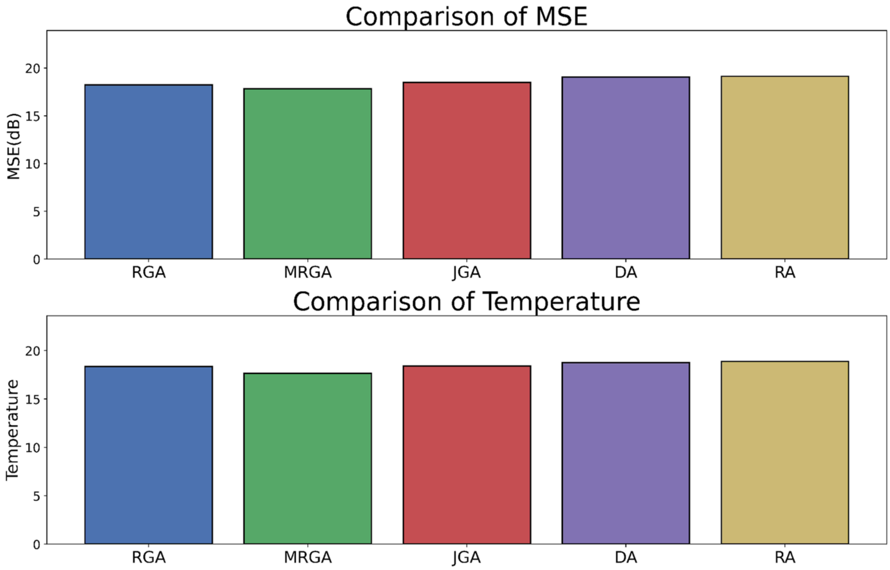

Fig. 6 Comparison chart of MSE and average temperature difference among the four algorithms in the large-scale fire detection scenarios

The quantitative results presented in Figure 6 further confirm these observations. In the large-scale setting, the MRGA achieves the lowest mean square error as well as the smallest average temperature deviation, followed by the RGA. In particular, the average temperature deviation produced by the MRGA is reduced by approximately 5.1% relative to that of the DA algorithm. These numerical findings are consistent with the visual patterns observed in the reconstructed fire scenes. Overall, the MRGA demonstrates both high accuracy and computational efficiency, making it a compelling choice for large-scale fire monitoring applications.

6 Conclusion

This paper investigates a measurement problem involving multiple groups of heterogeneous UAVs, where each group is constrained by a limited number of available units. The objective is to reduce estimation errors arising in linear inverse problems. To address this challenge, a submodular maximization algorithm is developed based on the weighted frame potential, and a rigorous upper bound for its performance is established. The proposed algorithm is evaluated in large-scale fire monitoring scenarios, where it demonstrates superior computational efficiency compared with existing methods. In addition, it achieves a reduction of approximately 5.1% in average estimation error in large-scale fire observations. In dynamic environments, UAV communication and coordination are crucial. Existing algorithms focus on minimizing measurement errors but overlook issues like communication delays and resource constraints during real-time deployment. As UAVs are reassigned in real time, factors like time-varying availability and environmental changes require continuous adjustments. To address these challenges, a reinforcement learning-based dynamic scheduling approach can be used to adjust UAV positions in real time, while leveraging distributed computing and parallelization to optimize coordination, reduce delays, and improve responsiveness.

Funding This work was partially supported by the Beijing Natural Science Foundation under Grant Nos. Z220004 and IS24001, and the National Natural Science Foundation of China under Grant No. 12571339.

Data Availability The data used in this study were randomly generated for the purpose of analysis and demonstration. No real-world datasets were used or analysed.

Declarations

Conflict of Interest The authors declare that they have no conflict of interest.

References

Alonso AA, Kevrekidis IG, Banga JR, Frouzakis CE (2004) Optimal sensor location and reduced order observer design for distributed process systems. Comput Chem Eng 28(1–2):27–35
Benedetto JJ, Fickus M (2003) Finite normalized tight frames. Adv Comput Math 18:357–385
Berger C, Wzorek M, Kvarnström J, Conte G, Doherty P, Eriksson A (2016) Area coverage with heterogeneous UAVs using scan patterns. IEEE international symposium on safety, security, and rescue robotics. pp 342–349
Bian F, Kempe D, Govindan R (2006) Utility based sensor selection. Proceedings of the 5th International Conference on Information Processing in Sensor Networks. ACM, Nashville Tennessee USA, pp 11–18
Chen J, Zhang Y, Wu L, You T, Ning X (2021) An adaptive clustering-based algorithm for automatic path planning of heterogeneous UAVs. IEEE Trans Intell Transp Syst 23(9):16842–16853
Chepuri SP, Leus G (2014) Sparsity-promoting sensor selection for non-linear measurement models. IEEE Trans Signal Process 63(3):684–698
Clark E, Askham T, Brunton SL, Kutz JN (2018) Greedy sensor placement with cost constraints. IEEE Sensors J 19(7):2642–2656
Conforti M, Cornuéjols G (1984) Submodular set functions, matroids and the greedy algorithm: tight worst-case bounds and some generalizations of the Rado-Edmonds theorem. Discret Appl Math 7(3):251–274
Fang Z, Savkin AV (2024) Strategies for optimized UAV surveillance in various tasks and scenarios: a review. Drones 8(5):1–41
Jamali-Rad H, Simonetto A, Leus G (2014) Sparsity-aware sensor selection: centralized and distributed algorithms. IEEE Signal Process Lett 21(2):217–220
Jiang C, Soh YC, Li H (2016) Sensor placement by maximal projection on minimum eigenspace for linear inverse problems. IEEE Trans Signal Process 64(21):5595–5610
Jiang C, Chen Z, Su R, Soh YC (2019) Group greedy method for sensor placement. IEEE Trans Signal Process 67(9):2249–2262
Joshi S, Boyd S (2008) Sensor selection via convex optimization. IEEE Trans Signal Process 57(2):451–462
Kay SM (1993) Fundamentals of statistical signal processing: estimation theory. Prentice-Hall, Inc
Krause A, Singh A, Guestrin C (2008) Near-optimal sensor placements in Gaussian processes: theory, efficient algorithms and empirical studies. J Mach Learn Res 9(2):235–284
Lee W, Bang H, Leeghim H (2013) Cooperative localization between small UAVs using a combination of heterogeneous sensors. Aerosp Sci Technol 27(1):105–111
Li B, Liu H, Wang R (2021) Efficient sensor placement for signal reconstruction based on recursive methods. IEEE Trans Signal Process 69:1885–1898
Liu S, Vempaty A, Fardad M, Masazade E, Varshney PK (2014) Energy-aware sensor selection in field reconstruction. IEEE Signal Process Lett 21(12):1476–1480

Liu L, Hua C, Xu J, Leus G, Wang Y (2023) Greedy sensor selection: leveraging submodularity based on volume ratio of information ellipsoid. IEEE Transactions Signal Process 71:2391–2406
Lv Y, Fan G, Li M, Liu X, Liu P, Zhang Y (2024) UAV target tracking with bandit-based data fusion. In: International Conference on Combinatorial Optimization and Applications, pp. 278-286. Beijing, China
Lv Y, Wu C, Xu D, Yang R, (2024) H-hop independently submodular maximization problem with curvature, High-Confidence Computing, **4**(3),
Majumder K, Pillai SRB, Mulleti S (2025) Greedy selection for heterogeneous sensors. IEEE Trans Signal Process 73:1394–1409
Mokhasi P, Rempfer D (2004) Optimized sensor placement for urban flow measurement. Phys Fluids 16(5):1758–1764
Nemhauser GL, Wolsey LA, Fisher ML (1978) An analysis of approximations for maximizing submodular set functions-I. Math Program 14:265–294
Ranieri J, Chebira A, Vetterli M (2014) Near-optimal sensor placement for linear inverse problems. IEEE Trans Signal Process 62(5):1135–1146
Rusu C, Thompson J, Robertson NM (2017) Sensor scheduling with time, energy, and communication constraints. IEEE Trans Signal Process 66(2):528–539
Shamaiah M, Banerjee S, Vikalo H (2010) Greedy sensor selection: Leveraging submodularity. 49th IEEE Conference on Decision and Control. IEEE, Atlanta, Georgia, USA, pp 2572–2577
Sultan L, Anjum M, Rehman M, Murawwat S, Kosar H (2021) Communication among heterogeneous unmanned aerial vehicles (UAVs): classification, trends, and analysis. IEEE Access 9:118815–118836
Welch WJ (1982) Branch-and-bound search for experimental designs based on D optimality and other criteria. Technometrics 24(1):41–48
Zhang P, Nevat I, Peters GW, Septier F, Osborne MA (2018) Spatial field reconstruction and sensor selection in heterogeneous sensor networks with stochastic energy harvesting. IEEE Trans Signal Process 66(9):2245–2257
Zhou H, Li X, Cher CY, Kursun E, Qian H, Yao SC (2012) An information-theoretic framework for optimal temperature sensor allocation and full-chip thermal monitoring. Proceedings of the 49th Annual Design Automation Conference. ACM, San Francisco, pp 642–647

Publisher's Note Springer Nature remains neutral with regard to jurisdictional claims in published maps and institutional affiliations.

Springer Nature or its licensor (e.g. a society or other partner) holds exclusive rights to this article under a publishing agreement with the author(s) or other rightsholder(s); author self-archiving of the accepted manuscript version of this article is solely governed by the terms of such publishing agreement and applicable law.